Electronic Supplementary Material (ESI) for Inorganic Chemistry Frontiers.

Supporting Information

Triggering synergistic electronic promoting effect through oxygen doping to promote electrochemical nitrogen reduction on metal-free electrocatalyst

Na Xu, Qiyang Cheng, Mengfan Wang,* Yanzheng He, Haoqing Ji,* Federico Rosei*

Methods

Synthesis of OENC, ONC, and NC. Typically, pyrrole was dispersed in deionized water, followed by the dissolution of ferrous chloride and sodium chloride. After adding 20 ml H_2O_2 to the solution, pyrrole polymerization was initiated. The solution was freeze-dried after vigorous stirring for 24 h. Then, the obtained material was placed in a ceramic boat and carbonized at 800 °C for 2 h under argon protection. After removing the salt through aqueous washing, the samples were dried under vacuum to obtain black powders. Finally, the materials were treated with hydrochloric acid and washed successively with deionized water and ethyl alcohol, and then dried in vacuum at 60 °C overnight to obtain OENC. ONC was fabricated through the same strategy as OENC, except changing the added H_2O_2 to 10 ml. NC was further prepared by annealing the ONC at 300 ℃ for 2 h in Ar/H_2 atmosphere.

Physical characterization. The morphology was investigated by a field emission scanning electron microscopy (FESEM, SU8010, Japan) and a field emission transmission electron microscopy (FETEM, FEI Tecnai G2 F20 S-TWIN TMP, Hong Kong). The catalyst was characterized by X-ray diffraction (XRD, D8 Advance, Bruker) and Raman spectroscopy (HR evolution, Horiba Jobin Yvon, France). Surface elemental analysis was performed on XPS (Kratos Axis Ultra Dld, Japan). N_2 sorption analysis was performed by an ASAP 2020 accelerated surface area and porosimetry instrument (Micromeritics) equipped with an automated surface area, using BET to calculate the surface area at 77 K.

Nitrogen purification. The $^{14}N_2$ commercially purchased from Messer Gas Product Co., Ltd. (99.999%) and $^{15}N_2$ commercially purchased from Newradar Special Gas Co., Ltd. (99 atomic% ^{15}N) were sequentially flowed through acid (0.1 M HCl), oxidising (0.1 M $KMnO_4$), and alkaline traps (0.1 M KOH) to remove possible contaminants, including NH_3, NO, and NO_2. Then, the gas was passed through a drying tube to prevent water vapour from entering the electrochemical cell.

Cathode preparation. First, 1 mg of catalyst was dispersed in 980 μl of ethanol, to which 20 μl of Nafion solution (5 wt.%) was added and sonicated for one hour. The mixed solution was used as homogeneous ink. Then, 50 μl of ink was evenly coated on

the carbon paper over an area of 1×1 cm^2 and dried at 80 °C for three hours. The obtained electrode was used for electrochemical measurements.

Electrochemical NRR measurements. The reduction of N_2 gas was carried out at room temperature in a two-chamber cell which was separated by a Celgard membrane with hydrophilic treatment. A three-electrode system was used for electrochemical measurements, with a carbon rod as the counter electrode and Ag/AgCl (4 M KCl) as the reference electrode. All measured potentials are converted to standard potentials versus RHE by calibration. The electrochemical impedance spectroscopy (EIS) measurements were carried out in a frequency range of 0.01 Hz-100 KHz. The electrical double layer specific capacitor (C_{dl}) of the materials were measured from double-layer charging curves using the cyclic voltammograms (CVs) in a small potential range. The plot current density against scan rate has a linear relationship and its slope is twice of C_{dl}. Purified N_2 was continuously fed into the cathode section at a certain flow rate of 30 sccm through a suitable sprayer, ensuring that the entire working electrode is in full contact with N_2 gas bubbles during the experiment. Electrochemical NRR reactions were carried out in N_2-saturated 0.1 M HCl at ambient temperature and pressure. The potentiostatic tests were carried at different potentials including -0.1, -0.2, -0.3, -0.4, -0.5 V vs. RHE. After the electrochemical reduction reaction, the electrolyte was collected and quantitatively analyzed either by colorimetric method or ^1H NMR spectroscopy.

Determination of ammonia in the electrolyte. NH_3 was determined by the indophenol blue method and NMR method. For indophenol blue method, 2 ml of the electrolyte was mixed with sodium hydroxide solution containing sodium citrate and salicylic acid (2 ml), followed by the addition of 0.05 M sodium hypochlorite (1 ml) and 1 wt.% sodium nitroferricyanide (0.2 ml). After 2 h, the absorption spectrum was measured using an ultraviolet-visible (UV-vis) spectrophotometer (UV-2700i, Shimadzu). The concentration-absorbance curves were calibrated using standard ammonium sulfate solution in 0.1 M HCl at a series of concentrations. For quantitative ^1H NMR measurements, various concentrations of ammonium sulfate were used to prepare the standard curve. The electrolyte was removed after electrolysis at -0.2 V vs. RHE. Then, the solution was concentrated to 0.5 ml and was mixed with 0.1 ml of

dimethylsulfoxide-d6. Maleic acid was used as the internal standard. The produced ammonia was quantified by using ^{1}H NMR spectroscopy (Agilent 600 MHz).

Determination of produced hydrazine. The hydrazine present in 0.1 M HCl was estimated by the Watt and Chrisp method. A mixture of para-(dimethylamino) benzaldehyde (5.99 g), HCl (concentrated, 30 ml), and ethanol (300 ml) was used as the chromogenic reagent. Next, 5 ml of the residual electrolyte after the NRR potentiostatic test was collected from the electrochemical reaction vessel. Then, 5 ml of the above prepared chromogenic reagent was added to the solution, and the mixture was stirred for 10 min at room temperature. The absorbance of the resulting solution was measured at a wavelength of 455 nm. The concentration-absorbance curves were calibrated using standard hydrazine monohydrate in 0.1 M HCl solution at a series of concentrations.

Determination of hydrogen evolution. HER test was performed with a CHI660E workstation by using a three electrode setup in a two-compartment cell at room temperature, to evaluate the HER performance of OENC, ONC, and NC in 0.1 M HCl. 1 × 1 cm^2 carbon paper loaded with catalyst was used as the working electrode. The carbon rod and Ag/AgCl (4 M KCl) electrode were used as the counter electrode and reference electrode, respectively. Before measurements, the electrolytes were saturated by N_2 for 30 min to remove O_2 impurity. The hydrogen production was measured within one second, when the current was stable. The H_2 was manual sampling and analyzed by gas chromatography (GC-2014, Shimadzu).

Faradaic efficiency and the yield rate. The Faradaic efficiency and yield rate of NH_3 were calculated as follows:

$$\text{Faradaic efficiency } (NH_3) = [3F \times c(NH_3) \times V] / Q \quad (1)$$

$$\text{Yield rate } (NH_3) = [17c(NH_3) \times V] / (t \times m) \quad (2)$$

where F is the Faraday constant (96,485 C mol^{-1}), t is the electrolysis time (1 h), m is the loading mass of the catalysts, Q is the total charge passed through the electrode, V is the volume of the electrolyte, and $c(NH_3)$ is the measured ammonia concentration.

The Faradaic efficiency of H_2 was calculated as below:

$$\text{Faradaic efficiency } (H_2) = [2 \times V_j \times P \times V \times 10^{-3} / RT] / [I_{total} \times t_H / F] \quad (3)$$

where V_j is volume percentage obtained from the GC analysis of H_2, P is the

atmospheric pressure (101.325 KPa), R is the gas constant (8.314 J mol^{-1} K^{-1}), V is the volume of sampling loop (1 cm^3), T is the temperature in Kelvin (298.15 K), I_{total} is the recording current, and t_H is the time required to fill the sampling loop.

^{15}N isotopic labeling experiment. After the electrolytic reaction, the obtained $^{15}NH_4^+$-contained electrolyte was collected. The generated $^{15}NH_3$ was quantified either by colorimetric method or ^1H NMR measurements (Agilent 600 MHz, USA) as that for $^{14}NH_3$.

DFT computational method and model. The first-principles calculations were conducted using the Vienna ab initio simulation package (VASP). The Perdew-Burke-Ernzerhof with generalized gradient approximation (GGA) was adopted to describe the electron-electron interaction. An energy cutoff of 450 eV was used, and a k-point sampling set of 3 × 3 × 1 was tested to be converged. The corresponding cell parameters are a = 14.760 Å, b = 14.760 Å, and c = 18.800 Å; α = 90°, β = 90°, and γ = 120°. The criterion for all structural optimizations was set to 10^{-5} eV for electronic energy convergence and Hellmann-Feynman force less than 0.01 eV $Å^{-1}$ for ionic relaxation loop. The vacuum space along the z-direction is set to be 15 Å. The Hubbard U correction was also employed within the DFT+U approach in all spin polarized calculations. The van der Waals dispersion forces was included using the zero damping DFT-D3 method of Grimme. The implicit solvent model, VASPsol, was applied to considered effects between the solute and solvent on the activation energies. The adsorption energy ΔE of the A group on the surface of the substrates was defined as:

$$E_{ads} = E_{*+intermediate} - E_{*} - E_{molecule} \quad (4)$$

where $E_{*+intermediate}$ and E_{*} are the energies of the surface with and without adsorbed molecules, respectively, and the $E_{molecule}$ is the energy of the molecule in the gas phase. Gibbs free energy change (ΔG) of each chemical reaction is calculated by:

$$\Delta G = \Delta E - T\Delta S + \Delta ZPE + \Delta G_{pH} \quad (5)$$

where ΔE is the total energy difference between reactants and products in a specific step, ΔZPE is the zero-point energy correction and ΔS is the entropy change in the reaction step. Here, T was set as room temperature (298.15 K). ΔG_{pH} is the contribution of H^+ and is equal to $-k_BT\times\ln(10)\times pH$, where k_B is the Boltzmann constant.

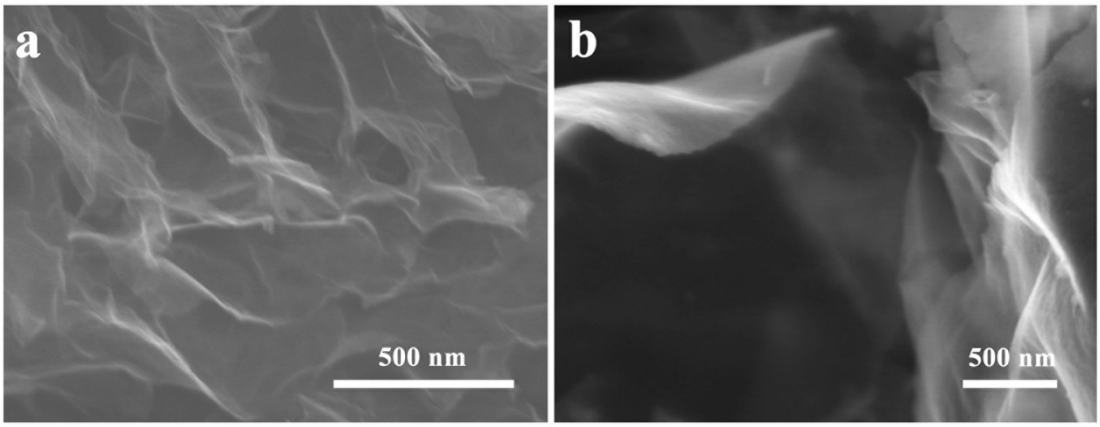

Fig. S1. Scanning electron microscopy images of (a) ONC and (b) NC.

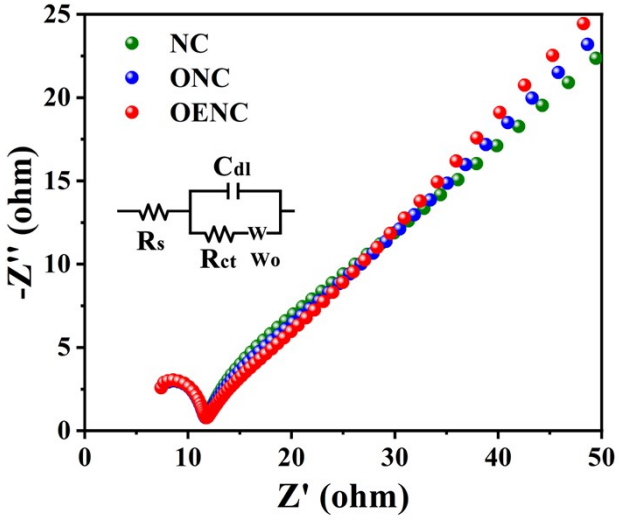

Fig. S2. Nyquist plots obtained using electrochemical impedance spectroscopy for the different electrodes, inset: the equivalent circuit used to fit the experiment data. Upon impedance spectra fitting, the charge transfer resistances (R_{ct}) are determined to be 5.983 Ω cm^{-2} for OENC, 5.937 Ω cm^{-2} for ONC, and 5.925 Ω cm^{-2} for NC.

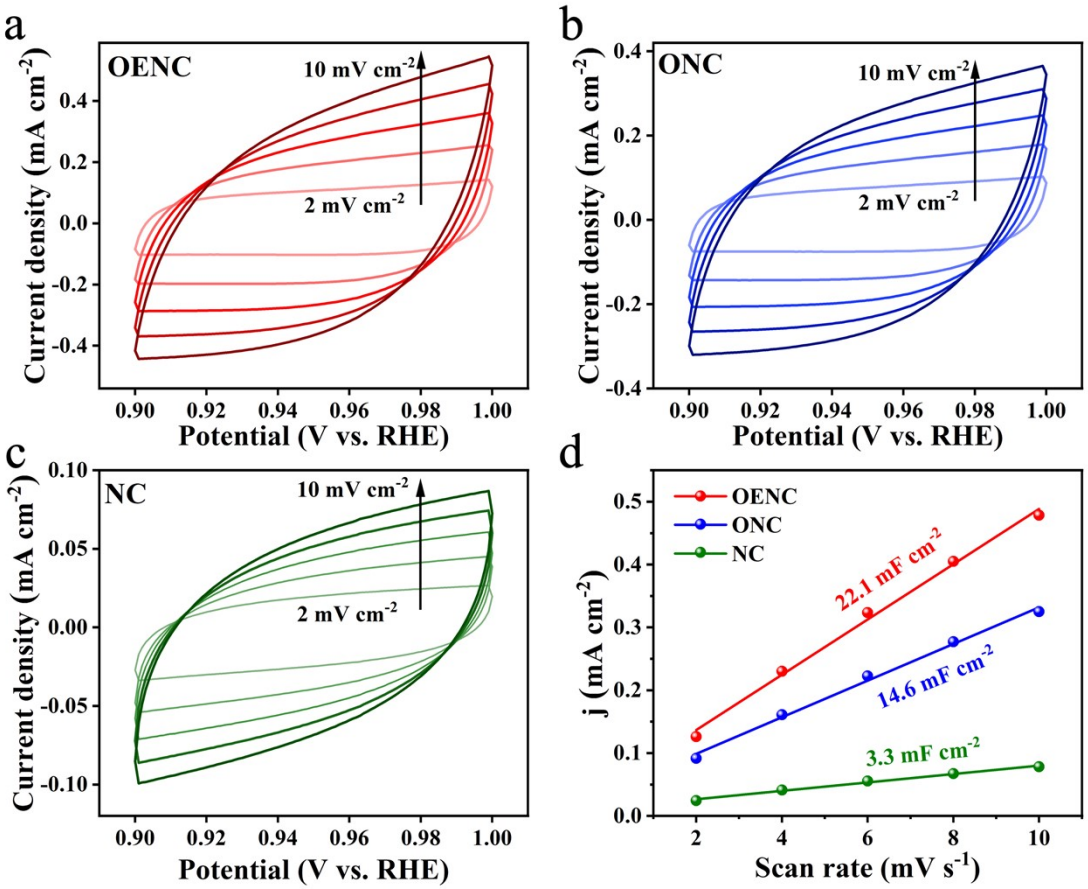

Fig. S3. Cyclic voltammograms of (a) OENC, (b) ONC, and (c) NC taken at different scan rates in a potential window where only double-layer charging and discharging occurs. (d) Double-layer charging current plotted against the CV scan rate for different electrodes.

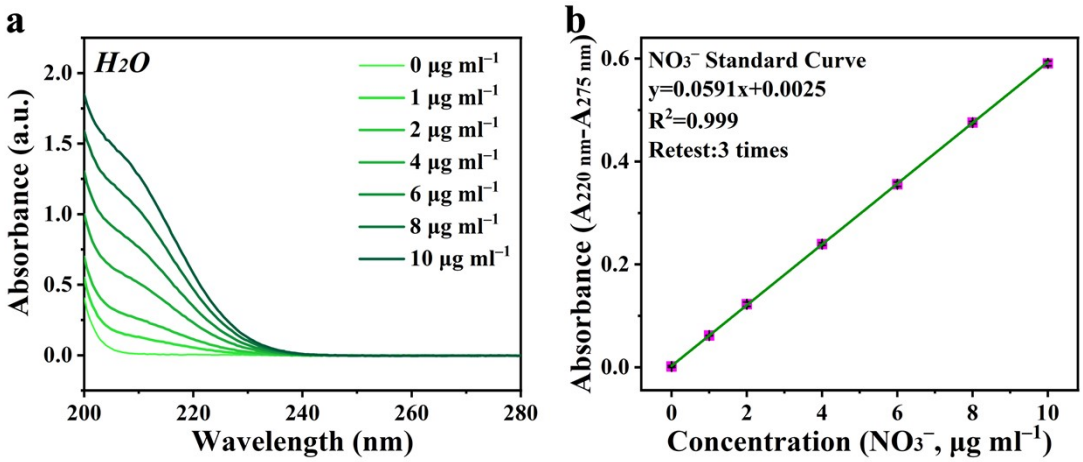

Fig. S4. (a) The UV-vis absorption spectra and (b) corresponding calibration curves for the colorimetric determination of NO_3^- in H_2O using the sulfamic acid method. The error bars correspond to the standard deviations of three separately prepared samples measured under identical conditions.

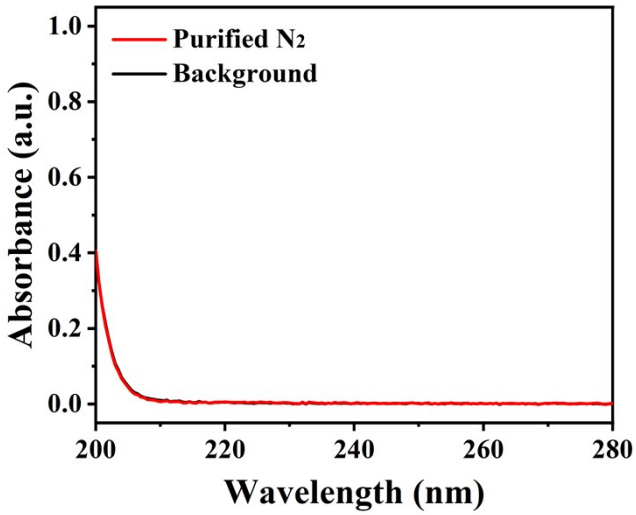

Fig. S5. The UV-vis absorption spectra of the H_2O background and the purified N_2 treated water using sulfamic acid method.

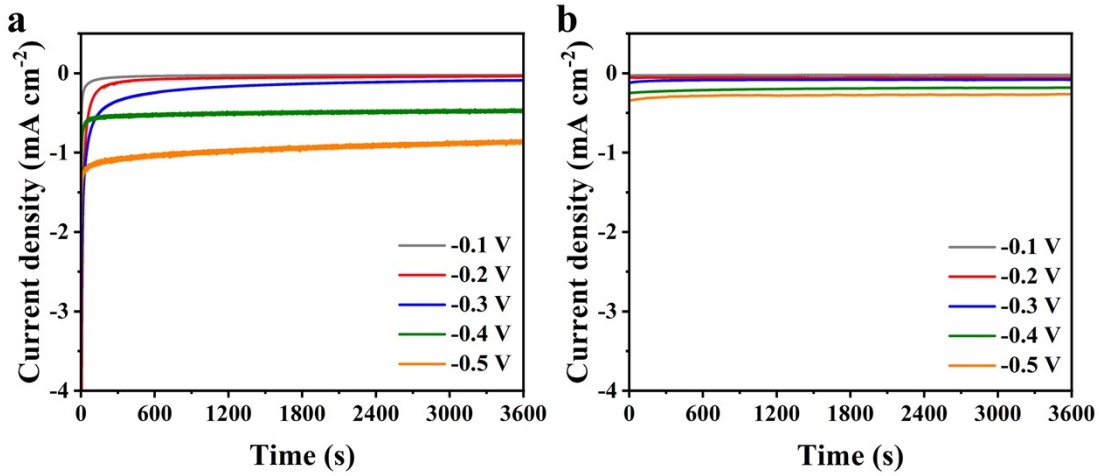

Fig. S6. Chronoamperometry results of (a) ONC and (b) NC tested in 0.1 M HCl at different applied potentials.

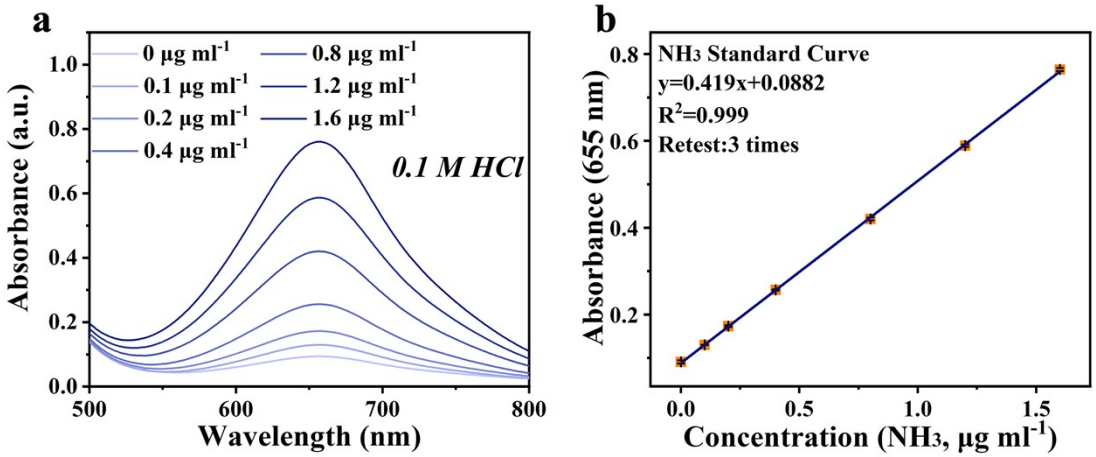

Fig. S7. (a) The UV-vis absorption spectra and (b) corresponding calibration curves for the colorimetric determination of NH_3 in 0.1 M HCl using the indophenol blue method. The error bars correspond to the standard deviations of three separately prepared samples measured under identical conditions.

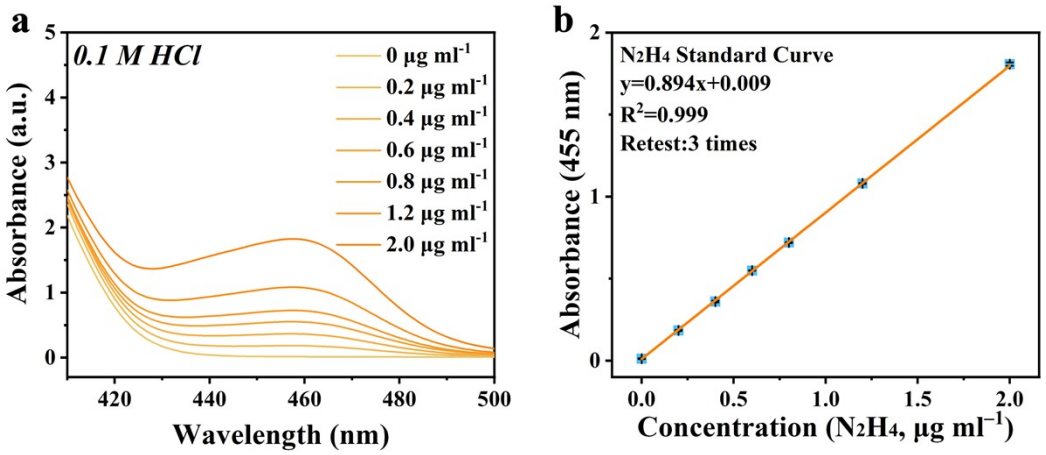

Fig. S8. (a) The UV-vis absorption spectra and (b) the corresponding calibration curves for colorimetric N_2H_4 determination in 0.1 M HCl using the Watt and Chrisp method. The error bars correspond to the standard deviations of three separately prepared samples measured under identical conditions.

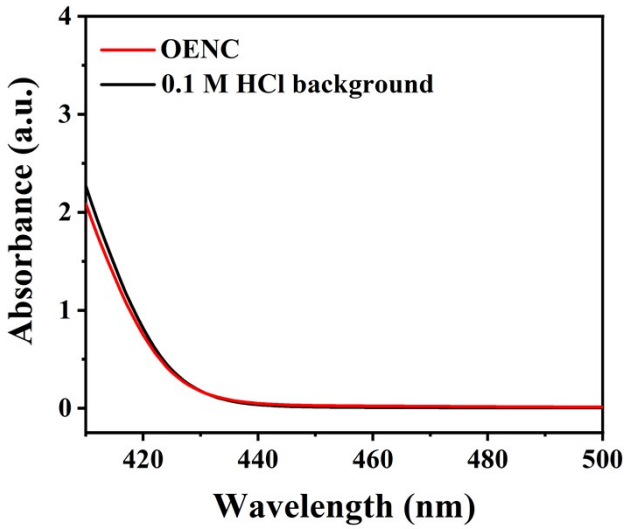

Fig. S9. The UV-vis absorption spectra of the electrolyte using the Watt and Chrisp method.

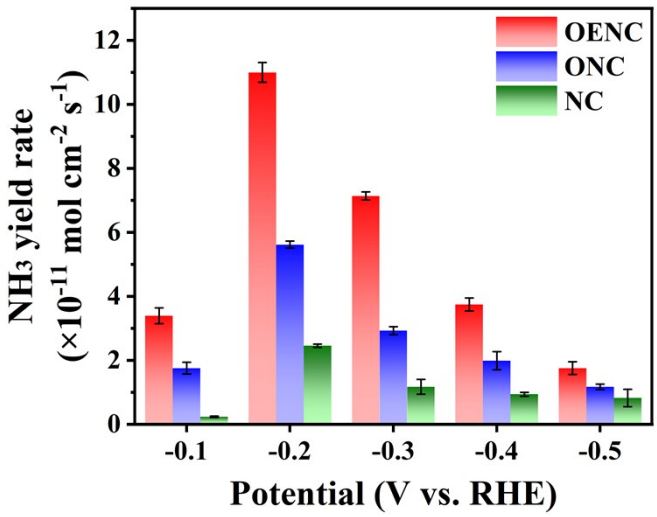

Fig. S10. NH_3 yield rates of OENC, ONC, and NC measured at all given potentials.

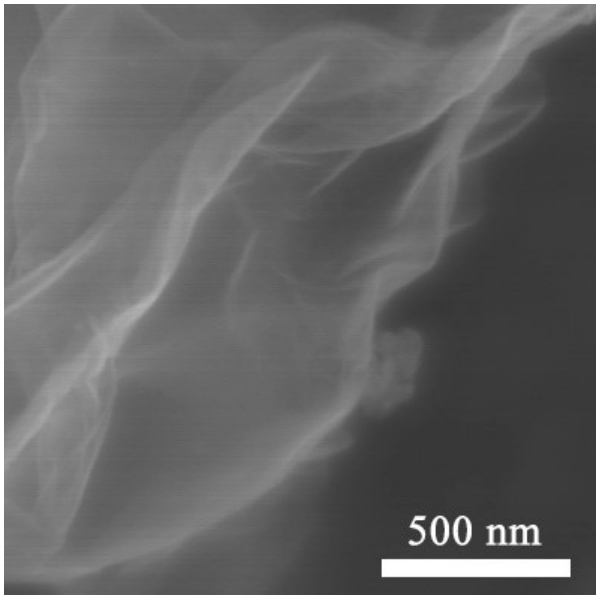

Fig. S11. Scanning electron microscopy image of the OENC after NRR electrolysis.

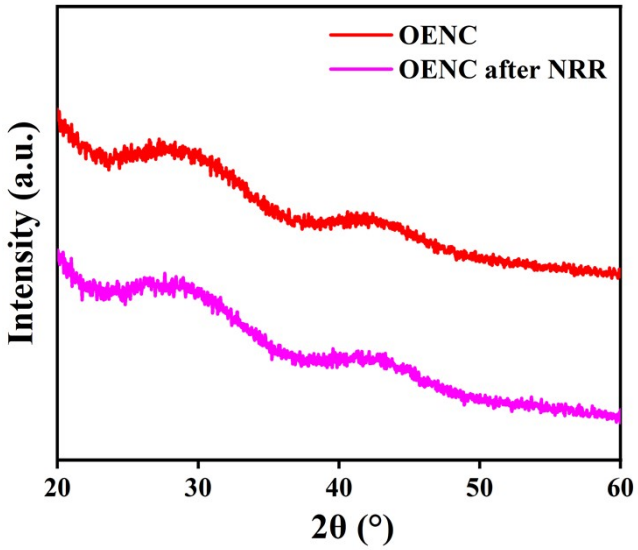

Fig. S12. XRD of the OENC after NRR electrolysis.

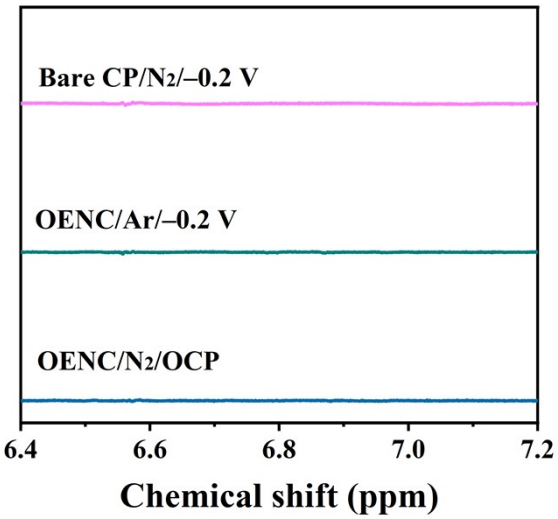

Fig. S13. ^{1}H NMR spectra of the electrolytes measured under different conditions.

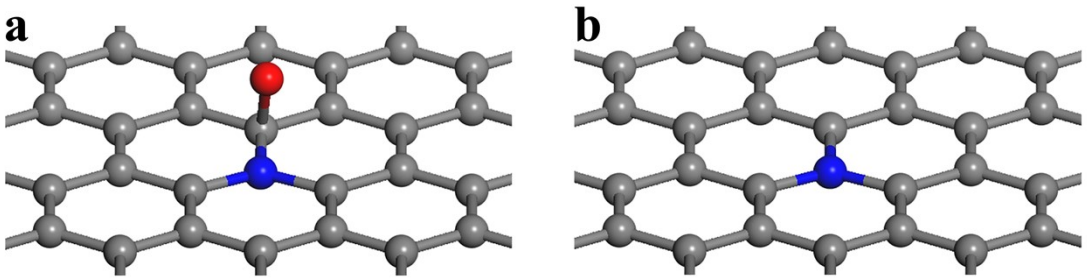

Fig. S14. The proposed configurations for computational studies of (a) O, N co-doped C and (b) N-doped C.

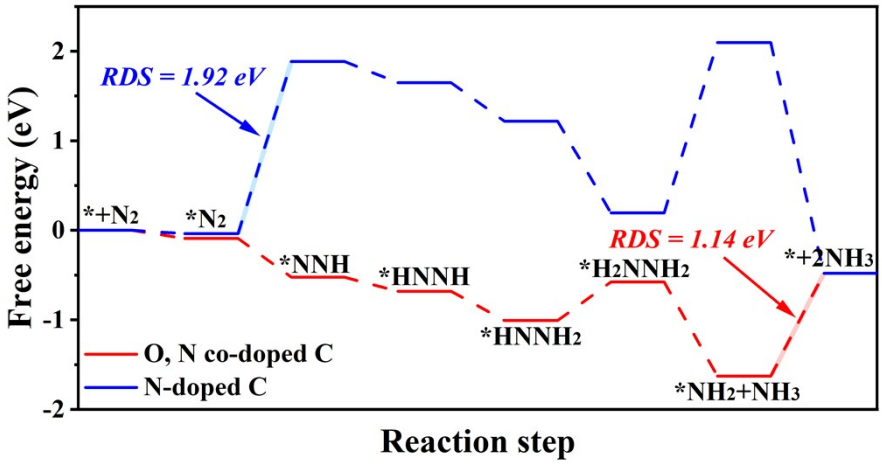

Fig. S15. Free energy diagram of the NRR on N-doped carbon and O, N co-doped carbon models through the alternating pathway.

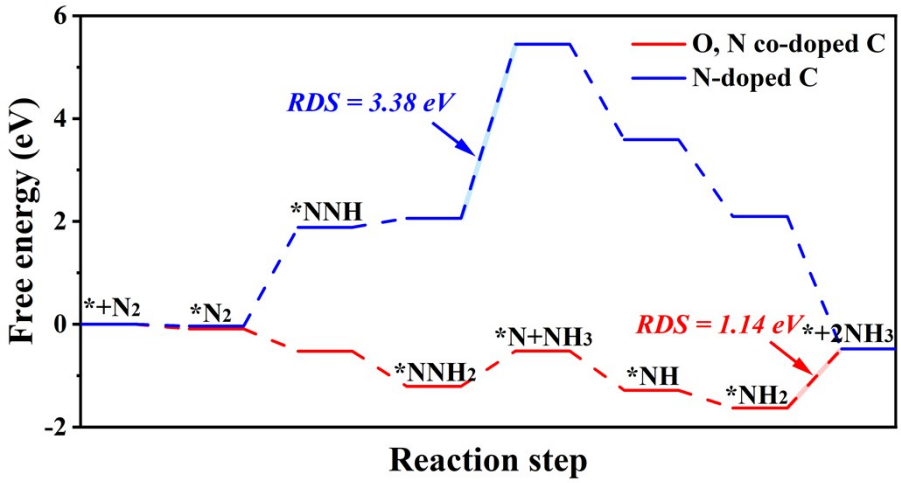

Fig. S16. Free energy diagram of the NRR on N-doped carbon and O, N co-doped carbon models through the distal pathway.

Table S1. Comparison of the electrocatalytic NRR performance at ambient conditions.

Catalyst	Electrolytre	Faradaic efficiency (%)	NH_3 yield rate ($\mu g\ h^{-1}\ mg–1\ cat$)	Ref.
ONC	0.1 M HCl	67.3	36.2	**This work**
Non-noble metal-based catalysts				
$Bi_4V_2O_{11}/CeO_2$	0.1 M HCl	10.16	23.21	[1]
Cr_2O_3 hollow microsphere	0.1 M Na_2SO_4	6.78	25.3	[2]
np-Mo_4P_3	0.1 M PBS	10.1	17.3	[3]
$BiVO_4$@MXene	0.1 M KOH	17.54	27.25	[4]
$Ni_{0.75}Fe_{0.25}Se_2$	0.1 M Li_2SO_4	12.3	8.4	[5]
Noble metal-based catalysts				
Pd/C	0.1M PBS	8.2	4.5	[6]
Au cluster/TiO_2	0.1 M HCl	8.11	21.40	[7]
$IrTe_4$	0.1 M KOH	14.4	26.2	[8]
Au–Fe_3O_4 Nanoparticles	0.1 M KOH	10.54	21.42	[9]
PdRu nanorod	0.1 M HCl	2.40	34.20	[10]
Metal-free catalysts				
PEBCD	0.5 M Li_2SO_4	2.9	1.2	[11]
Defect-rich fluorographene nanosheets	0.1 M Na_2SO_4	4.2	9.3	[12]
CN_xB_y	0.1 M HCl	10.58	16.40	[13]
NPC-500	0.005 M H_2SO_4	10.0	22.3	[14]
Metal-free polymeric carbon nitride	0.1 M HCl	11.59	8.09	[15]

Reference

[1] C. Lv, C. Yan, G. Chen, Y. Ding, J. Sun, Y. Zhou, G. Yu, An amorphous noble-metal-free electrocatalyst that enables nitrogen fixation under ambient conditions, Angew. Chem. Int. Ed. 57 (2018) 6073-6076, https://doi.org/10.1002/anie.201801538.

[2] Y. Zhang, W. Qiu, Y. Ma, Y. Luo, Z. Tian, G. Cui, F. Xie, L. Chen, T. Li, X. Sun, High-performance electrohydrogenation of N_2 to NH_3 catalyzed by multishelled hollow Cr_2O_3 microspheres under ambient conditions, ACS Catal. 8 (2018) 8540-8544, https://doi.org/10.1021/acscatal.8b02311.

[3] L. Xiao, S. Zhu, Y. Liang, Z. Li, S. Wu, S. Luo, C. Chang, Z. Cui, Effects of hydrophobic layer on selective electrochemical nitrogen fixation of self-supporting nanoporous Mo_4P_3 catalyst under ambient conditions, Appl. Catal. B-Environ. 286 (2021) 119895, https://doi.org/10.1016/j.apcatb.2021.119895.

[4] D. Zhang, S. Yang, X. Fang, H. Li, X. Chen, D. Yan, In situ localization of $BiVO_4$ onto two-dimensional MXene promoting photoelectrochemical nitrogen reduction to ammonia, Chinese Chem. Lett. 33 (2022) 4669-4674, https://doi.org/10.1016/j.cclet.2022.02.001.

[5] S. Yang, W. Ye, D. Zhang, X. Fang, D. Yan, Layered double hydroxide derived bimetallic nickel–iron selenide as an active electrocatalyst for nitrogen fixation under ambient conditions, Inorg. Chem. Front. 8 (2021) 1762-1770, https://doi.org/10.1039/D0QI01437K.

[6] J. Wang, L. Yu, L. Hu, G. Chen, H. Xin, X. Feng, Nat. Commun. 9 (2018) 1795.

[7] M.-M. Shi, D. Bao, B.-R. Wulan, Y.-H. Li, Y.-F. Zhang, J.-M. Yan, Q. Jiang, Au sub-nanoclusters on TiO_2 toward highly efficient and selective electrocatalyst for N_2 conversion to NH_3 at ambient conditions, Adv. Mater. 29 (2017) 1606550, https://doi.org/10.1002/adma.201606550.

[8] H. Wang, J. Wang, R. Zhang, C. Cheng, K. Qiu, Y. Yang, J. Mao, H. Liu, M. Du, C. Dong, X. Du, Bionic Design of a Mo(IV)-Doped FeS_2 Catalyst for Electroreduction of Dinitrogen to Ammonia, ACS Catal. 10 (2020) 4914–4921, https://doi.org/10.1021/acscatal.0c00271.

[9] J. Zhang, Y. Ji, P. Wang, Q. Shao, Y. Li, X. Huang, Adsorbing and activating N_2 on heterogeneous Au–Fe_3O_4 nanoparticles for N_2 fixation, Adv. Funct. Mater. 30 (2019) 1906579, https://doi.org/10.1002/adfm.201906579.

[10] H. Wang, Y. Li, D. Yang, X. Qian, Z. Wang, Y. Xu, X. Li, H. Xue, L. Wang,

Direct fabrication of bi-metallic PdRu nanorod assemblies for electrochemical ammonia synthesis, Nanoscale 11 (2019) 5499-5505, https://doi.org/10.1039/C8NR10398D.

[11] G. F. Chen, X. Cao, S. Wu, X. Zeng, L. X. Ding, M. Zhu, H. Wang, Ammonia Electrosynthesis with High Selectivity under Ambient Conditions via a Li^+ Incorporation Strategy, J. Am. Chem. Soc. 139 (2017) 9771–9774, https://doi.org/10.1021/jacs.7b04393.

[12] J. Zhao, J. Yang, L. Ji, H. Wang, H. Chen, Z. Niu, Q. Liu, T. Li, G. Cui, X. Sun, Defect-rich fluorographene nanosheets for artificial N_2 fixation under ambient conditions, Chem. Commun. 55 (2019) 4266-4269. https://doi.org/10.1039/C9CC01920K.

[13] J.-T. Ren, C.-Y. Wan, T.-Y. Pei, X.-W. Lv, Z.-Y. Yuan, Promotion of electrocatalytic nitrogen reduction reaction on N-doped porous carbon with secondary heteroatoms, Appl. Catal. B-Environ. 266 (2020) 118633, https://doi.org/10.1016/j.apcatb.2020.118633.

[14] C. Zhao, S. Zhang, M. Han, X. Zhang, Y. Liu, W. Li, C. Chen, G. Wang, H. Zhang, H. Zhao, Ambient Electrosynthesis of Ammonia on a Biomass-Derived Nitrogen-Doped Porous Carbon Electrocatalyst: Contribution of Pyridinic Nitrogen, ACS Energy Lett. 4 (2019) 377–383, https://doi.org/10.1021/acsenergylett.8b02138.

[15] C. Lv, Y. Qian, C. Yan, Y. Ding, Y. Liu, G. Chen, G. Yu, Defect engineering metal-free polymeric carbon nitride electrocatalyst for effective nitrogen fixation under ambient conditions, Angew. Chem. Int. Ed. 57 (2018) 10246-10250, https://doi.org/10.1002/anie.201806386.